Volume 9
Number 7
July 2024
Pages 1055–1220

Nanoscale Horizons

The home for rapid reports of exceptional significance in nanoscience and nanotechnology

rsc.li/nanoscale-horizons

ISSN 2055-6756

ROYAL SOCIETY OF CHEMISTRY

COMMUNICATION

Vasudevanpillai Biju, Yuta Takano *et al.*
Bio-catalytic nanoparticle shaping for preparing mesoscopic assemblies of semiconductor quantum dots and organic molecules

NCNST

Nanoscale Horizons

ROYAL SOCIETY OF CHEMISTRY

COMMUNICATION

View Article Online
View Journal | View Issue

Cite this: *Nanoscale Horiz.*, 2024, 9, 1128

Received 28th March 2024,
Accepted 13th May 2024

DOI: 10.1039/d4nh00134f

rsc.li/nanoscale-horizons

Bio-catalytic nanoparticle shaping for preparing mesoscopic assemblies of semiconductor quantum dots and organic molecules†

Rumana Akter,‡[a] Nicholas Kirkwood,[b] Samantha Zaman,[b] Bang Lu,[ac] Tinci Wang,[a] Satoru Takakusagi,[ac] Paul Mulvaney,[b] Vasudevanpillai Biju *[ad] and Yuta Takano ‡*[ad]

We report a unique bio-catalytic nanoparticle shaping (BNS) method for preparing a variety of mesoscopic particles by a facile process. For example, the BNS method affords mesoscopic QD assembly dispersions. Large-size sedimentations (>1 μm) of QDs are first formed using oligo-L-lysine linkers. These then undergo controlled enzymatic cleavage of the linkers using trypsin, which surprisingly leads to mesoscopic particles about 84 nm in size with a narrow size distribution. A detailed mechanism of the BNS method is investigated using tetrakis(4-carboxyphenyl)porphyrin (TCPP), instead of QDs, as a probe molecule. Interestingly, the BNS method can also be applied to other combinations of enzymes and enzymatically degradable linkers, such as hyaluronidase with hyaluronan. As a potential application, the mesoscopic particles of QDs and oligo-lysine exhibit their ability to act as a drug delivery carrier originating from the features of both QDs and oligo-lysine. The BNS method demonstrates the universality and versatility of preparing mesoscopic particles and opens new doors for studying QD assemblies and molecular-based mesoscopic particles.

New concepts

In this study, we have developed an unprecedented method, which we call the bio-catalytic nanoparticle shaping (BNS) method, to obtain mesoscopic assembly dispersions by a facile process. The key point of this method, quite different from prior methodologies, is the use of controlled enzymatic cleavage for large sedimentations. Interestingly, the BNS method can be applied to various combinations of enzymes and compounds with enzymatically degradable linkers, such as trypsin and oligo-L-lysine, or hyaluronidase with hyaluronan. The core compounds can be organic and inorganic materials. This study provides valuable knowledge for a novel, universal, and versatile approach to preparing mesoscopic particles. Because of the high flexibility and variety of bio-enzymes, the potential of the BNS method is enormous, as it can create functional particles composed of quite a wide variety of materials. Also, the present concept of "bio-catalytic nanoparticle shaping" will inspire researchers to develop various nanoparticles using bio-catalysts.

1. Introduction

Quantum dots (QDs) have demonstrated great potential in advanced materials,[1] including solar cells, quantum computing, and bio-imaging.[2–4] When these materials are brought to a size comparable to the exciton Bohr radius, they exhibit size-dependent optical absorption.[5–7] Research on QDs accelerated with the invention of soluble QDs by synthesizing colloidal QDs.[8,9] These materials enabled the production of high-quality QDs with narrow size distribution and high uniformity. Colloidal QDs can be easily processed and integrated into devices, making them particularly useful for applications in optoelectronics and bio-imaging.[1–4,10] Because of its great potential to enrich our lives and technologies, the inventors of QDs were awarded the Nobel Prize in 2023.[5,8,11]

Intermolecular interactions among QDs have gathered attention for revealing and utilizing the full potential of QDs based on their unique electronic and quantum properties. For instance, the optical and electronic properties of QD assemblies can be tuned by the size of the individual quantum dots and the spatial arrangement and inter-dot distances in the assembly.[12–14] These assemblies opened up new possibilities for the design and fabrication of high-density data storage devices,[15] building blocks for molecular computation,[16] photocatalysts,[17] and solar cells with enhanced efficiency.[18] Very recently, Tahara and co-workers reported unprecedented upconversion properties of QD assemblies fabricated on a substrate, showing the great potential of QD assemblies for next-generation materials.[19]

[a] *Graduate School of Environmental Science, Hokkaido University, Sapporo 0600810, Japan. E-mail: biju@es.hokudai.ac.jp, tak@es.hokudai.ac.jp*
[b] *ARC Centre of Excellence in Exciton Science, School of Chemistry, The University of Melbourne, Parkville, Victoria, 3010, Australia*
[c] *Institute for Catalysis, Hokkaido University, Sapporo 0010021, Japan*
[d] *Research Institute of Electronic Science, Hokkaido University, Sapporo 0010020, Japan*

† Electronic supplementary information (ESI) available. See DOI: https://doi.org/10.1039/d4nh00134f

‡ These authors contributed equally.

Although the study of QD assembly is very worthwhile and has great potential, a limited number of methods are available for preparation.[20–23] In particular, it is still rare to find methods for preparing soluble/dispersible QD assemblies consisting of a significant number of (typically over ten) QDs,[24–26] even though multiple QDs exhibit concerted and outstanding effects.[12–19] Although the reported methods are available, they require the use of an appropriate scaffold or precise control of reaction conditions to avoid undesirable sedimentation of the QD assembly in a large size. Therefore, universal and versatile methods to obtain soluble/dispersible QD assemblies have been desired.

In this study, we develop a biocatalytic nanoparticle shaping (BNS) method that uses hydrolytic enzymes to prepare various mesoscopic particles composed of QDs or, alternatively, organic molecules. Bio-catalytic reactions, including enzymatic reactions, are universally seen in organic/inorganic chemical syntheses for bonding, cleaving, degradations, and biological reactions. The advantages of bio-catalytic reactions are their variety and selectivity. For example, trypsin, one of the most widely used enzymes in biology, selectively cleaves the amide bond in a lysine or an arginine residue.[27–29] Hyaluronidase specifically cleaves the glycosidic bond in hyaluronan.[30] There are a variety of enzymes for cleaving peptide-bond (peptidase), glycosidic bond (glycosidase), ester bond (esterase), *etc.* However, these enzymatic reactions have been rarely applied to the preparation of functionalized QDs.[31]

In the present case, the BNS method is utilized to prepare mesoscopic particles of QDs (**ms-QD**) or an organic molecule, tetrakis(4-carboxyphenyl)porphyrin (TCPP), linked by oligo-L-lysine chains by a simple mixing and centrifugal process with trypsinization. The size of the mesoscopic particles ranges from several to hundreds of nanometers. Mesoscopic particles exhibit unrivaled properties in a wide range of fields, owing to the combined or synergistic nature of quantum and bulk effects,[32–35] such as drug delivery in medicine,[36] catalysis with high specific surface area,[37] and photoelectric conversion with efficient carrier transport.[38] The reaction with TCPP is employed to study a detailed mechanism in the formation of mesoscopic particles. The use of amino-substituted porphyrin, tetrakis(4-aminophenyl)porphyrin (TAPP), reveals the versatility of the BNS method, demonstrating its capacity to involve the other combinations instead of lysine and trypsin. Furthermore, **ms-QD** shows excellent luminescence derived from the constituent QDs of **ms-QD** at the single particle level, and cell adhesion and internalization ability derived from the positively charged oligo-lysine moiety. As shown in this example, the BNS method demonstrates the potential to create a variety of functional mesoscopic particles.

2. Experimental section

General

All chemicals used in this study were of analytical grade and used as received. 4-(4,6-Dimethoxy-1,3,5-triazin-2-yl)-4-methylmorpholinium chloride (DMT-MM), ethanol (EtOH, anhydrous, >98%), (polyethylene glycol) methyl ether thiol was purchased from Sigma-Aldrich, Japan. L(+)-Lysine monohydrochloride, 0.5 w/v% trypsin-5.3 mmol L^{-1} EDTA were obtained from FUJIFILM Wako Pure Chemical Corporation, Japan. 3,3,3′,3′-Tetramethyl-1,1′-bis(4-sulfobutyl)benzoindodicarbocyanine sodium salt (sulfo-Cy5.5) was from Tokyo Chemical Industry, Japan. HS-PEG3500-COOH and HO-PEG3000-COOH were from Nanosoft Biotechnology LLC, NC, USA. Solvents in reagent grade were provided by FUJIFILM Wako Pure Chemical Corporation, Japan.

UV-vis absorption spectra were obtained by absorption spectrometers (Evolution 220, Thermo Fisher Scientific, USA, or UV-1900i, Shimadzu, Japan). The steady-state fluorescence spectra were recorded by a fluorescence spectrometer (RF-6000, Shimadzu, Japan). DLS data was measured by nanoSAQLA (Ohtsuka Electronics, Japan). STEM Hitachi HD-2000 ultra-thin film observation at 200 kV was used to analyze the shape and size. For this technique, carbon-coated STEM Cu100P grids were used. The Quantaurus-Tau (Hamamatsu Photonics, Japan) was used to measure the PL lifetimes. FT-IR spectra were recorded on a JASCO FT/IR-6800typeA spectrometer equipped with a diamond-enabled attenuated total reflectance (ATR) sample holder (JASCO, Japan).

Synthesis of COOH functionalized CdSe/CdS QD (QD-COOH)

The starting CdSe/CdS QDs were prepared according to our previous report[39] and characterized with the data therein. CdSe/CdS QD (10.0 mg) in chloroform (10.0 mg) was taken in a glass tube. HS-PEG3500-COOH (11.4 nmol) and HO-PEG3000-COOH (46.1 nmol) were mixed well in 1.0 mL chloroform. Then, this mixture was added to the QD solution and sonicated for 3 min. The mixture was kept on the heat shaker at 25 °C and 1000 rpm overnight. A clear solution was obtained, and hexane was added gradually for precipitation. After that, centrifugation was performed at 10 000 g. The upper part was discarded, and the precipitate was collected and repeatedly washed. The solvent was evaporated at a reduced pressure, and **QD-COOH** was obtained as a yellow solid.

Synthesis of the mesoscopic quantum dot assembly (ms-QD)

QD-COOH (5.0 mg) was sonicated in EtOH, and DMT-MM (0.411 mmol) was added to activate the COOH group. L-Lysine (0.137 mmol) was added to the solution and sonicated for 3 min. The solution in a glass tube was then placed on a heat shaker for 12 hours at 40 °C and 1000 rpm. Then, the precipitate was collected and washed three times with water by centrifugation at 5000 g. The solvent was replaced with 10 mM HEPES aq. 1.0 mL of trypsin solution (0.5 wt%) was added to the dispersion and placed on a heat shaker for 12 h at 40 °C and 1000 rpm. The precipitate was then collected by centrifugation at 15 000 g for 10 min and washed three times with water. The solvent was evaporated at a reduced pressure, and **ms-QD** was obtained as a yellow solid (yield. 45.6 wt%). **ms-QD** was dispersed in 5.0 mL of water and used for experiments.

FT-IR (ATR): ν 3230, 2394, 1748, 1638, 1524, 1392, 1255, 1050, 1004, 970, 854, 798, 706 cm^{-1}.

Synthesis of the monomeric quantum dot (mono-QD)

QD-COOH (5.0 mg) was taken and sonicated in EtOH. DMT-MM (0.227 μmol) was added and well mixed by sonication. Following that, L-lysine (0.103 μmol) was added, thoroughly mixed, and sonicated. After that, the mixer was placed in a heat shaker for 12 h at 1000 rpm and 40 °C. The precipitate was collected by centrifugation at 30 000 g for 30 min and then washed twice with water. The solvent was evaporated at a reduced pressure, and **mono-QD** was obtained as a yellow solid. **mono-QD** was dispersed in 5.0 mL of water and used for experiments.

Synthesis of the mesoscopic TCPP assembly (ms-TCPP)

To a tetrakis(4-carboxyphenyl)porphyrin (TCPP) solution of DMSO, 16, 64, 254, or 520 eq. of DMT-MM was added. To the solution, 4, 16, 64, or 254 eq. of L-lysine was added respectively and sonicated for 3 min, followed by shaking in a heat shaker for 5 h at 50 °C and 400 rpm. The formed precipitates were collected and washed repeatedly with water by centrifugation at 5000 g. The solvent was replaced with 10 mM HEPES aq. To the dispersion, trypsin solution (50 wt% of trypsin to L-lysine) was added. The mixture was placed on a heat shaker for 12 h, set to 45 °C and 1000 rpm. The precipitate was then centrifuged at 25 000 g for 10 min and washed repeatedly with water. The solvent was evaporated at a reduced pressure, and **ms-TCPP** was obtained as a brown solid (yield. 16.4 wt% in the case of **ms-TCPP64**).

FT-IR (ATR) for **ms-TCPP64**: ν 3370, 3316, 2930, 1750, 1646, 1638, 1598, 1580, 1544, 1468, 1364, 1312, 1230, 1176, 1116, 1096, 1016, 968, 866 cm^{-1}.

X-ray photoelectron spectroscopy (XPS)

XPS measurements were conducted with the TX400 X-ray source and RESOLVE 120 spectrometer (PSP Vacuum Technology Ltd, UK) under 8×10^{-8} Pa. The Mg-K_α (1253.6 eV) line was used as an X-ray source. The X-ray source emission current was set to 15 mA, while its voltage was set to 12 KV. The samples were pressed and embedded onto Indium film on a copper plate. The binding energies (BE) were calibrated by In 3d5/2 of In_2O_3 set at 443.8 eV.

$^1O_2$ generation ability assays

ms-TCPPs or **rTPA@ms-QD** dispersion was taken in 700 μL of 10 mM HEPES aq. and 4.0 μL of 1.0 mM SOSG solution was added. PL spectra (WL_{ex}: 450 or 490 nm, WL_{em}: 550 nm) were recorded after an NIR light irradiation (Xe lamp, 700 nm, 50 nm bandpass, 50 mW cm^{-2}).

Synthesis of the mesoscopic TAPP assembly with hyaluronan (ms-TAPP/HA)

To a tetrakis(4-aminophenyl)porphyrin (TAPP) solution of DMSO, hyaluronan (64 eq. of the units to TAPP) and DMT-MM (150 eq.) mixed solution of water were added. The solution was sonicated for 3 min, followed by shaking in a heat shaker for 5 h at 50 °C and 400 rpm. The formed precipitates were collected and washed repeatedly with water by centrifugation at 5000 g. The solvent was replaced with 50 mM MES aq. A hyaluronidase solution (50 wt% of hyaluronidase to L-lysine) was added to the dispersion. The mixture was placed on a heat shaker for 12 h, set to 45 °C and 1000 rpm. The precipitate was then centrifuged at 30 000 g for 10 minutes and washed repeatedly with water. Thus, **ms-TAPP/HA** was obtained as an orange solid.

Preparation of ms-QD and rTPA conjugate (rTPA@ms-QD)

2.0 mg of **ms-QD**s in 10 mM HEPES was taken in a tube. 0.2 mg **rTPA** in DMSO was added to the **ms-QD**s dispersion. The mixture was then left overnight at room temperature on a heat shaker with 1000 rpm. Then, the sample was centrifuged at 20 000 g and precipitated. The precipitation was washed twice with water and dispersed in 1.00 mL of 10 mM HEPES aq. and used for assays.

A reference compound **rTPA@mono-QD** was prepared by the same procedure, using **mono-QD** instead of **ms-QD**.

Cell culture

HeLa cells were obtained from the RIKEN cell bank, and cultured in 10% fetal bovine serum (FBS)-Dulbecco's modified Eagle's minimal essential medium (DMEM) with low glucose, additional complement with penicillin and streptomycin. Cells were cultured in a 37 °C incubator with 5% CO_2/air. The cell passages were performed at 80–90% confluency.

Imaging of the spheroids of HeLa by a one-photon and two-photon laser microscope

The samples were observed by a multiphoton excitation microscope (A1R-MP, Nikon, Japan) equipped with a silicone oil immersion objective lens (PLAN APO W 25x NA1.05, SIL, Nikon, Japan). The correction rings were aligned to maximize the fluorescence intensity of the sample. 405 nm CW-laser or 800 nm pulsed laser light (120 fs, 80 MHz) was used to excite the sample. Dichroic mirrors were used to detect luminescence from the sample with a signal range of 601–657 nm.

Cell viability assays on the spheroid using an ATP detection kit

200 μL of HeLa cell culture medium suspension containing 4000 cells was dropped into each well of a 96-well plate designated for spheroid preparation (MS-9096U, Sumitomo Bakelite, Japan). The plates were covered with lids and incubated for 48 hours at 37 °C in a 5% CO_2. Then, the culture solution was changed to 100 μL of DMEM (FBS−) and transfected with **rTPA** or **rTPAs@ms-QD** for 30 min, followed by 24h incubation in DMEM (FBS+), and then illuminated using a xenon lamp (MAX-303, Asahi Spectra; Tokyo, Japan) with a band pass filter (700 nm bandpass 50 nm, 200 mW cm^{-2}). The cells were incubated for 24 h at 37 °C. 100 μL of KATAMARI ATP assay solution ver 2.1 (Toyo B-Net. Japan) was added to the spheroids. The photoluminescence (PL) was measured using a plate reader Varioskan (Thermo Fischer, co., USA). Assays were performed in triplicate, and the results were analyzed statistically using GraphPad Prism and a one-way ANOVA, followed by Tukey's multiple comparison test for significance. The viabilities were

calculated using the following equation (eqn (1)).

$$\text{Cell viability (\%)} = \frac{\text{PL}_{\text{sample}} - \text{PL}_{\text{blank}}}{\text{PL}_{\text{control}} - \text{PL}_{\text{blank}}} \quad (1)$$

3. Results and discussion

Formation of mesoscopic assemblies of QDs by the BNS method

In the present study, we anticipated that when quantum dots form large aggregates ($d > 1000$ nm), trypsin may enzymatically cleave the oligo-L-lysine chains that connect the quantum dots to form smaller particles. To demonstrate that this is possible, large assemblies were first prepared from colloidal CdSe/CdS QDs capped by SH-PEG3500-COOH (**QD-COOH**), followed by amide-condensation reaction using DMT-MM with a large amount of mono-lysine (400 wt% to **QD-COOH**) (Fig. 1A). This reaction yielded microscale precipitates, confirmed by dynamic light scattering (DLS) (Fig. S1, ESI†). The precipitate was treated with trypsin at 40 °C for 12 hours, and well-dispersed mesoscopic quantum dot assemblies (**ms-QDs**) were obtained. A reference compound of monomeric quantum dots (**mono-QDs**) was also prepared for comparison to have a better understanding of the properties of **ms-QD**. DLS measurements indicated that **QD-COOH**, **ms-QD**, and **mono-QD** particles were well-dispersed in an aqueous solution with mean hydrodynamic sizes of 8.6 ± 4.8, 84.4 ± 22.1 nm, and 22.6 ± 4.0 nm respectively (Fig. 1B–D), with narrow size-distribution verified by their small poly-dispersibility index (<0.2). Thus, the size of **ms-QD** was sure to be on the mesoscopic scale, typically 30–200 nm.

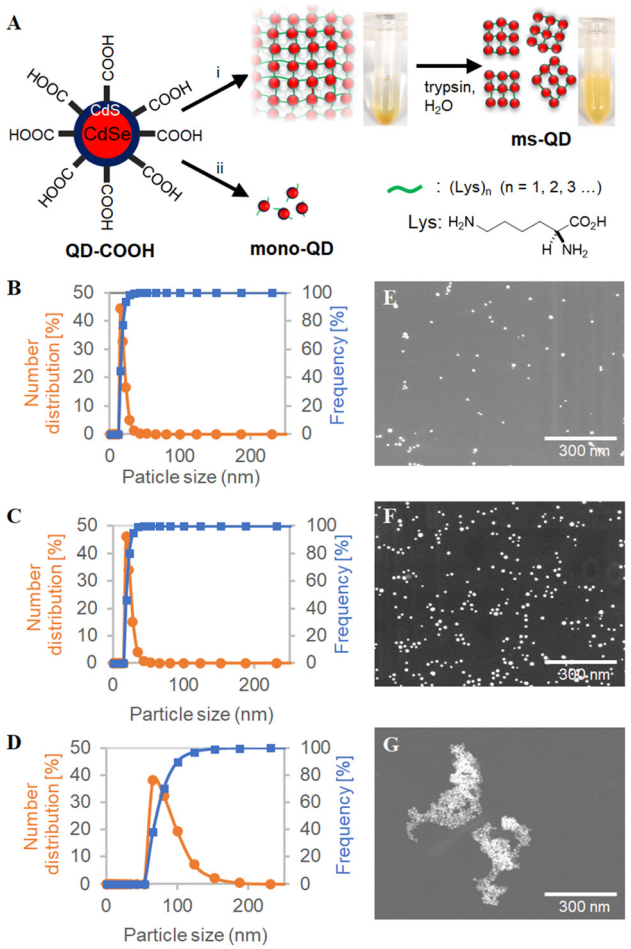

Fig. 1 (A) Synthetic scheme to prepare **ms-QD** by the BNS method, and a reference compound, **mono-QD**. (i) 400 wt% (to **QD-COOH**) L-lysine, DMT-MM, 40 °C, 12 h, in water, (ii) 0.30 wt% (to **QD-COOH**) L-lysine, DMT-MM, 40 °C, 12 h, in water. Inset photos show the corresponding dispersions. The DLS profiles of (B) **QD-COOH**, (C) **mono-QD**, and (D) **ms-QD** in 10 mM HEPES aq., and the STEM images of (E) **QD-COOH**, (F) **mono-QD**, and (G) **ms-QD**.

The scanning transmission electron microscopic (STEM) observations also confirmed that **ms-QD** was mesoscopic assemblies and **mono-QD** and **QD-COOH** were monomeric QDs, respectively (Fig. 1E–G). The morphology of **ms-QD** was unique, and cross-linked aggregates appeared to form several layered sheets (Fig. 1G and Fig. S2, ESI†). This structure implies a plausible mechanism of particle formation, in which partial and incomplete enzymatic cleavage of the amide bonds in the oligo-lysine chains forms the aggregates to be mesoscopic particles. FT-IR spectra of **ms-QDs** indicated the presence of the amide bonds in such oligo-lysine chains as characteristic amide bands at 1638, 1524, 1255 cm^{-1} (Fig. S3, ESI†). The layered structure would form spherical **ms-QDs** by solvation and self-assembly in an aqueous solvent. The incomplete enzymatic cleavage may be led by the bulkiness of the QD blocking the interaction between the substance and the enzyme.

Absorption spectra revealed that **QD-COOH**, **ms-QD**, and **mono-QD** absorb light from 600 nm to the UV region (Fig. 2A–C). **ms-QD** exhibits light scattering signals, which were not seen in **QD-COOH** and **mono-QD**, over 600 nm due to its relatively large particle size.[40] The photoluminescence (PL) spectra demonstrated the 645, 645, and 650 nm peaks for QD-COOH, **mono-QD**, and **ms-QD** under 405 nm photoexcitation (Fig. 2D and E). The red-shifted and weaker emission of **ms-QDs** relative to **mono-QD** indicated an internal emission-reabsorption process in the assembly.[41] This feature will be promising for fabricating novel optical materials utilizing energy or electron/hole transfer processes with proper optimization in future studies.

Particle formation mechanism by the BNS method and its potential

To further investigate the mesoscopic particle formation process and essential factors of the BNS method, mesoscopic particles of tetrakis(4-carboxyphenyl)porphyrin (TCPP) and oligo-lysine (**ms-TCPP**) were synthesized and studied in several reaction conditions (Fig. 3A). A porphyrin analog, TCPP, was chosen because its optical, electronic, and photophysical properties are sensitive to the surrounding environment, making it suitable as a probe.[42–44] A series of **ms-TCPP** were prepared by changing the ratio of starting TCPP and lysine molecules in the 1 : 4, 1 : 16, 1 : 64, and 1 : 256 ratios (mol : mol) to prepare large

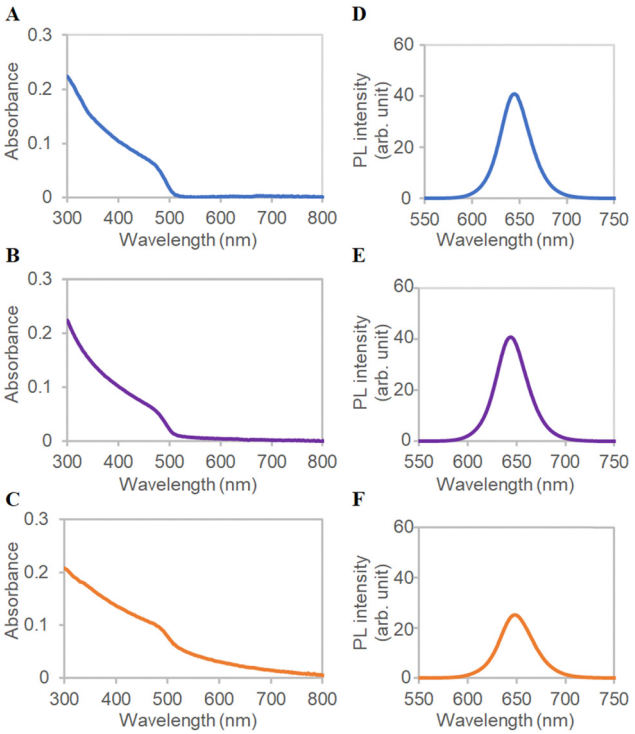

Fig. 2 Absorption spectra of (A) **QD-COOH**, (B) **mono-QD**, and (C) **ms-QD**, and photoluminescence (PL) spectra (λ_{ex}: 405 nm) of (D) **QD-COOH**, (E) **mono-QD**, and (F) **ms-QD** in 10 mM HEPES aq. The absorbances at the excitation wavelengths were set to be identical (0.20) for all samples.

sedimentations (Fig. 3A). These conditions correspond to 1, 4, 16, and 64 lysine moieties between two TCPP units in the assembly at the maximum inclusion of lysine. After the amide-condensation reactions using DMT-MM, all conditions afforded visible sedimentation as the result of multiple-amidation. Notably, the following trypsinization gave mesoscopic particles except for 1 : 4 and 1 : 16 (denoted as **ms-TCPP4** and **ms-TCPP16**). The particle sizes of **ms-TCPP4** and **ms-TCPP16** were large and on a micro meter scale (>5000 nm), as shown by the DSL measurements (Fig. S4 and Table S1, ESI†). This result indicates that the lysine linkers formed in these conditions, probably consisting of one to four lysine molecules, are too short to be accessed by trypsin for enzymatic cleavage.

This fact is supported by the similarity of the absorption spectra of **ms-TCPP4** and **ms-TCPP16**, especially the strongest Soret band (407 nm), which suggests a similar environment around the porphyrin unit.[45,46]

Meanwhile, the condition with the higher composition of lysine moieties (*i.e.*, 1 : 64, and 1 : 256) followed by trypsinization afforded well-dispersed **ms-TCPP64** and **ms-TCPP254**, as evidenced by the DLS profiles showing their mesoscopic particle sizes (94.2 and 81.4 nm, respectively) (Fig. S4 and Table S1, ESI†). FT-IR spectra of **ms-TCPP64** demonstrated characteristic amide bands at 1638, 1544, and 1230 cm^{-1} (Fig. S3, ESI†). X-ray photoelectron spectroscopy (XPS) also indicated amide bond formations with the peak at 401 eV, along with the presence of amino moieties appeared at 400 eV,[47] in **ms-TCPP64** (Fig. S5, ESI†). The different mesoscopic particle formation results for **ms-TCPP64** and **ms-TCPP254** from those for **ms-TCPP4** and **ms-TCPP16** implied that more than four lysine moieties between two porphyrin moieties are necessary to cleave the oligo-lysine chains and form the mesoscopic particles effectively. Although the molecular size of a single TCPP is not as large as QDs, it may be enough to intercept the substance/enzyme interaction. The structural flexibility of trypsin and **ms-TCPP** would allow access to the peptide chain that is cleaved at the enzymatic reaction site of trypsin. In the absorption spectral measurements, **ms-TCPP64** and **ms-TCPP256** demonstrated different spectra from **ms-TCPP4** and **ms-TCPP16**, especially the red-shift in the most intense Soret band (439 nm for **ms-TCPP64** and 444 nm for **ms-TCPP254**). In the present case, the different absorption spectra of the **ms-TCPPs** indicated the different environments around the core units, TCPP, depending on the introduced oligo-lysine linker length.

To shed light on the difference among **ms-TCPPs** depending on their structures, singlet oxygen ($^1O_2$) generation assays were performed. $^1O_2$ is useful for various applications, such as photocatalysts and photo-therapeutic cancer drugs.[46,48] In TCPP and its derivatives, $^1O_2$ is formed as the result of photo-induced energy transfer from the excited porphyrin core to molecular oxygen ($^3O_2$), which can be detected using a commercial fluorogenic $^1O_2$ sensor, singlet oxygen sensor green (SOSG).[49,50]

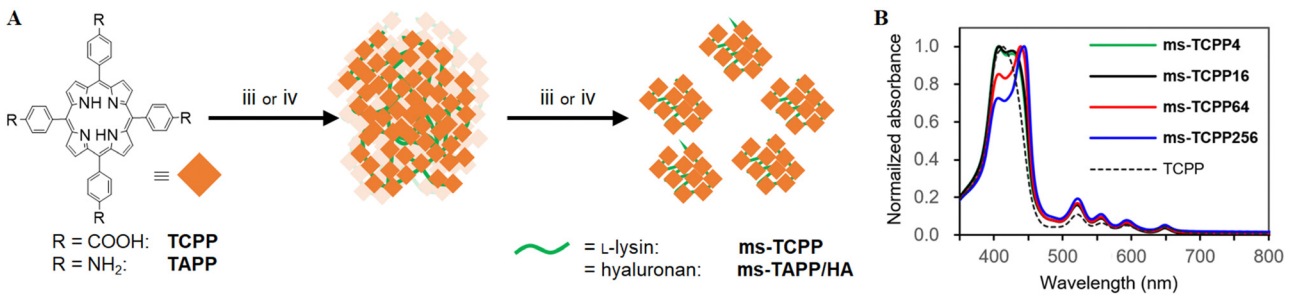

Fig. 3 (A) Synthetic scheme of mesoscopic particle preparation. (iii) For **ms-TCPP**; L-lysine, DMT-MM, 50 °C, 3 h, in water, then trypsin, 40 °C, 15 h, in water. (iv) For **ms-TAPP/HA**; hyaluronan, DMT-MM, 50 °C, 3 h, in water, then hyaluronidase, 45 °C, 15 h, in 50 mM MES aq. (B) Normalized absorption spectra of **ms-TCPP** prepared in the various conditions and a pristine TCPP in 10 mM HEPES aq.

Notably, **ms-TCPP64** showed the largest production of $^1O_2$ among **ms-TCPPs** (Fig. S6, ESI†). This result indicates that an optimized lysine composition would efficiently maximize the photosensitizing ability of **ms-TCPP**. This may be caused by a good balance of the oligo-lysine length that avoids undesired aggregation of the porphyrin core, which reduces the efficiency of photoreaction by shortening the photoexcited state lifetime and suppressing efficient energy funneling in the particle.[44] Consequently, the BNS method evidenced its potential to tune and modulate the molecular function of the core units of the particles by changing the composition of the linker molecules.

It is noteworthy that the present BNS method is also applicable to other combinations of enzymes and substrates. Using tetrakis(4-aminophenyl)porphyrin (TAPP) as the core unit instead of TCPP, its combination with hyaluronan also yielded the corresponding mesoscopic particles. In this case, hyaluronidase, which is a hyaluronan-selective glycosidase,[30] demonstrated its effectiveness for the BNS method to form corresponding mesoscopic particles, **ms-TAPP/HA**, which possess the averaged hydrodynamic size of 200 nm (Fig. S7, ESI†). Absorption spectra of **ms-TAPP/HA** show characteristic absorption bands of the porphyrin moiety around 430 and 660 nm (Fig. S7C, ESI†). These results demonstrate the applicability of BNS to a wide variety of enzymes and enzymatically cleavable structures. This fact indicates the universality and versatility of the method for preparing solvent-dispersible mesoscopic particles from both organic and inorganic materials.

One more important finding is that a control experiment using trypsin, which is not a matched cleaving enzyme to hyaluronan, did not give mesoscopic particles with a narrow size distribution (Fig. S7E, ESI†). This result guarantees that the particle formation mechanism of the BNS method is not based on the dispersant effect caused by the proteins,[51] which have been reported for various proteins, such as albumin acting like a dispersant,[52] but on the effective enzymatic cleavage, as mentioned above. The cleavage may afford both the mesoscopic-sized particles directly and further cleaved fragments which possess smaller sizes than the particles. As the fragments generally consist of amphiphilic moieties (*e.g.*, QDs-Lys$_n$, TCPPs-Lys$_n$, and TAPPs-HA in the present cases), these fragments in small sizes are probably unstable in the aqueous solvent and prefer to form self-assembled particles in a specific size and distribution.[53]

Intermolecular interaction and energy transfer properties of ms-QD

For application development of the products by the BNS method, photophysical properties of **ms-QD** were investigated. As **ms-QD** demonstrated distinct particle size, absorption, and emission properties from **mono-QD**, Förster resonance energy transfer (FRET) behavior was examined to reveal the abilities of **ms-QD**.[54] Here, sulfo-Cy5.5 and a π-extended porphyrin, **rTPA**,[46,48] were used as the FRET acceptors (Fig. S8, ESI†). Sulfo-Cy5.5 was anticipated to show FRET due to its absorption spectral matching with the emission of **ms-QD**. **rTPA** was selected because it should demonstrate less FRET efficiency than sulfo-Cy5.5 and achieve an independent photosensitizing effect, as discussed later. To the dispersion of **ms-QD** in HEPES buffered solution, sulfo-Cy5.5 was added step-wise. Remarkably, the absorbance around 405 nm, mainly originating from the QD moiety, decreased as the sulfo-Cy5.5 concentration increased (Fig. 4A and C). In particular, a sharp decrease was observed at the initial addition steps (0 to 0.1 μM). DLS measurements explained the cause of the decrease in absorbance. The hydrodynamic size of **ms-QD** was 121 nm in the absence of sulfo-Cy5.5, whereas the size decreased with increasing the concentration of sulfo-Cy5.5 from 0.005 μM to 0.5 μM, by 121 to 78 nm (Fig. S9, ESI†). This result implied that the particles shrunk when sulfo-Cy5.5 was added. A feasible explanation for this shrinking is that negatively charged sulfo-Cy5.5 molecules gather the positively charged lysine moieties in **ms-QD**, and then the clearance space among the molecules in the particles is reduced, causing the shrinkage. It was reported for the nanoparticles that the decrease of the clearance space causes the decrease of optical cross-section and, thus, the optical density of the nanoparticles.[55] This would be applicable to the present case of **ms-QD** and sulfo-Cy5.5. Meanwhile, the PL intensities and lifetimes decreased with increasing concentrations of sulfo-Cy5.5 (Fig. 4B and C). Because the PL decrease was much larger than the absorbance decrease, the PL quench was feasibly caused by an electronic interaction between them. A new PL peak from sulfo-Cy5.5 was found around 721 nm in the PL spectra, indicating the interaction was FRET from QD to sulfo-Cy5.5.

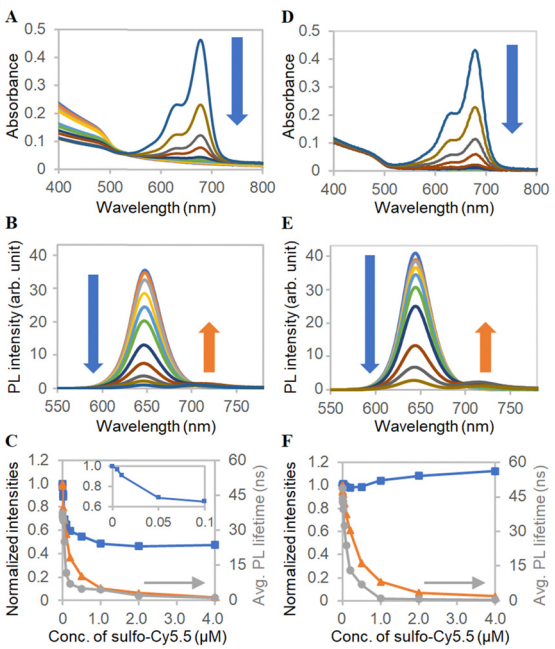

Fig. 4 FRET analysis with sulfo-Cy5.5. (A) Absorption spectra and (B) PL spectra of **ms-QD** with various concentrations of sulfo-Cy5.5, which are indicated in the *x*-axis of Fig. 4C. (C) Concentration-dependent profiles of normalized (blue) absorbance at 405 nm of Fig. 4A, (orange) PL intensity at 650 nm of Fig. 4B and (grey) averaged PL lifetimes. Inset shows the absorbance at a low concentration range. (D)–(F) Corresponding data to Fig. 4A–C obtained with **mono-QD** and sulfo-Cy5.5.

FRET was also investigated for **mono-QD** with sulfo-Cy5.5. The PL intensities and lifetimes dropped with the increase in the concentration of sulfo-Cy5.5, indicating that FRET also presents in the case of mono-QD and sulfo-Cy5.5 (Fig. 4E and F). In contrast with **ms-QD**, the absorbance did not decrease. The increase was caused by the absorption of sulfo-Cy5.5 at the high concentration and the light scattering increase, as mentioned below. It was found that the particle size of **mono-QD** increased drastically with increasing concentrations of the additive, sulfo-Cy5.5, and did not maintain a monodisperse state with uniformly isolated particles (Fig. S10, ESI†). This caused light scattering because of the large particle size. This result implies that the decrease in absorbance in **ms-QD** was indeed due to shrinkage, which did not happen in **mono-QD**. Moreover, **mono-QD** is not stable against the addition of additives, such as sulfo-Cy5.5. In contrast, **ms-QD** is stable for adding and probably incorporating the additives. This feature of **ms-QD** is beneficial as a drug delivery system (DDS) carrier, as discussed in the following section.

To further investigate the intermolecular interactions of **ms-QD**, we employed a π-extended porphyrin, **rTPA**,[46,48] which possesses the absorption band in longer wavelength (half-maxima 665–735 nm) than sulfo-Cy5.5 (half-maxima 620–695 nm) (Fig. S8A, ESI†). The addition of **rTPA** to **ms-QD** decreased its absorbance (Fig. 5A and C) due to contraction, as in the case of sulfo-Cy5.5, because of the negatively charged nature of **rTPA**. The size of **ms-QD** decreased to 70 nm with **rTPA**. Meanwhile, a difference from sulfo-Cy5.5 was found in the PL intensities and lifetimes change. **rTPA** did not change them vastly (Fig. 5B), indicating a weak interaction between **rTPA** and **ms-QD** that has little effect on the PL properties of **ms-QD**. A similar trend was observed in **mono-QD**. This result suggests that photoinduced energy or electron transfers do not happen remarkably in the combination of **rTPA** and **ms-QD**. Maintaining the luminescent property of ms-QD and the photoactive property of **rTPA** is beneficial.

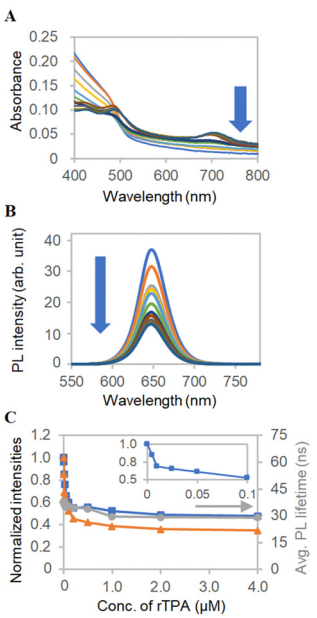

Fig. 5 FRET analysis with **rTPA**. (A) Absorption spectra and (B) PL spectra of **ms-QD** with various concentrations of **rTPA**, which are indicated in the *x*-axis of Fig. 5C. (C) Concentration-dependent profiles of normalized (blue) absorbance at 405 nm of Fig. 5A, (orange) PL intensity at 650 nm of Fig. 5B and (grey) averaged PL lifetimes. The inset shows the absorbance at a low concentration range.

Mesoscopic particles prepared by the BNS method for a drug carrier

As described above, the discovery of the unique mesoscopic particle size and maintenance of the luminescent properties of **ms-QD** when encapsulated with certain types of compounds drove us to develop a DDS that is based on **ms-QD**. This DDS enabled us to track the location of **ms-QD** in a living system. A conjugate of **msQD** and **rTPA** was prepared by simply mixing them to be the conjugate (**rTPA@ms-QD**) *via* an electric charge interaction. Remarkably, the luminescence intensity of **rTPA@ms-QD** was much stronger than that of **rTPA@mono-QD** at the single-particle level because **ms-QD** is composed of numbers of QDs (Fig. 6A and B). It is worth mentioning that **ms-QD** can luminesce both single-photon excitation and two-photo excitation, as expected from the nature of QDs (Fig. S11, ESI†).[56] Singlet oxygen generation ($^1O_2$) ability of **rTPA@ms-QD** was assessed using SOSG. The result indicated that **rTPA@ms-QD** possesses a $^1O_2$ generation ability under 700 nm light irradiation, which selectively photoexcites **rTPA** in **rTPA@ms-QD** (Fig. 6C).[46,48] The $^1O_2$ generation ability was larger than that of pristine **rTPA** in the aqueous solution. This result implied that **rTPA** moieties were well distributed in **ms-QD**, suppressing undesired aggregation of **rTPA**, which decreases $^1O_2$ generation ability.[48]

The above results guaranteed that **rTPA@ms-QD** possesses both abilities of bright photolabeling and photoinduced $^1O_2$ generation, which is useful for medical applications of photo-mediated cancer or bacterial killing.[46,57] Thus, **rTPA@ms-QD** was tested in a spheroid, a living cellular assembly consisting of more than hundreds of cells that mimic realistic tissues.[58] Because spheroids are usually much thicker specimens than conventionally cultured cells on a dish, higher luminescence is required to clearly visualize the photo label under microscopic observations. In this regard, a two-photon laser microscope successfully visualized **rTPA@ms-QD** in a spheroid of HeLa cells (Fig. 6D). A key point of successful internalization and visualization of **rTPA@ms-QD** in the cells can be the original nature of oligo-lysine, which has a high affinity to the cell membrane and helps with cellular uptake.[59] An NIR-light illumination on **rTPA** in **rTPA@ms-QD** evidenced a cancer-killing effect on the spheroids, confirmed by ATP assays (Fig. 6E). Although 20 μg of **rTPA@ms-QD** induced 33% cell death in the spheroids and was not high enough to destroy the cancer cells, this result is meaningful to demonstrate the potential of **ms-QD** as a DDS carrier in the three-dimensional cell system, such as spheroids, with maintaining the photo-activity of the cargo, **rTPA** in the present case. Further development in the particles prepared by the BNS method will

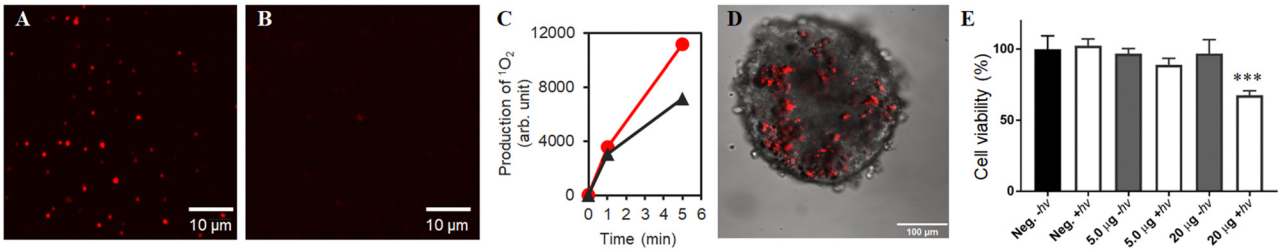

Fig. 6 Two-photo laser microscopic images (λ_{ex}: 800 nm) of (A) **rTPA@ms-QD** and (B) **rTPA@mono-QD** on a glass coverslip under the identical excitation laser power at 800 nm and detector sensitivity on the best focus. (C) Singlet oxygen assays of (red circle) **rTPA@ms-QD** and (black triangle) **rTPA** using SOSG under illumination (Xe lamp, 700 ± 25 nm bandpass filter, 50 mW cm^{-2}). (D) Two-photo laser microscopic image (λ_{ex}: 800 nm) of **rTPA@ms-QD** (red signals) in a spheroid of HeLa cells. (E) ATP-mediated cell viability assays of the spheroids treated with **rTPA@ms-QD** and illumination (Xe lamp, 700 ± 25 nm bandpass filter, 5 min, 200 mW cm^{-2}). A statistically significant difference from the negative control is illustrated with asterisks (***$P < 0.001$).

achieve more effective luminescent drug delivery carriers in the future.

4. Conclusions

In the present study, a unique method using bio-catalysts, named the BNS method, has been developed to shape and form various mesoscopic particles consisting of inorganic nanomaterials, QDs, and organic molecules, peptides and porphyrins, as the components. A combination of QD and oligo-lysine afforded water-dispersible mesoscopic-sized **ms-QD**, with a hydrodynamic size of around 84 nm. **ms-TCPP**, which consists of organic molecules, TCPP and oligo-lysine, demonstrated the feasible mechanism of the particle formation by the BNS method and its potential. This method allows us to use various enzymes for BNS methods, such as in the case of **ms-TAPP/HA**, which consists of porphyrins and hyaluronic acid. As an example of an application, the combination of organic/inorganic materials, **rTPA** and QD, based on oligo-lysine moieties achieves the design and construction of a noble luminescent DDS carrier (**rTPA@ms-QD**). This system utilizes unique mesoscopic-sized properties and has demonstrated cancer-killing ability in spheroids. Most remarkably, both the core (**rTPA** or **ms-QD**) and the linker (oligo-lysine) moieties offer the functionalities of the mesoscopic particles. Therefore, the potential of the BNS method is enormous, and can be used to create functional particles composed of quite a wide variety of materials. We believe the BNS method opens new doors for dispersible inorganic/organic assemblies, including semiconducting QDs.

Author contributions

R. A.: data curation, writing – original draft, writing – review & editing, investigation. N. K.: resources, writing – review & editing. S. Z.: resources, writing – review & editing. B. L.: data curation, writing – review & editing. T. W.: data curation. S. T.: data curation, resources, writing – review & editing. P. M.: resources, writing – review & editing. V. B.: resources, funding acquisition, writing – review & editing, supervision. Y. T.: conceptualization, funding acquisition, data curation, writing – original draft, writing – review & editing, investigation, supervision, project administration.

Conflicts of interest

Y. T. is the inventor of patent application JP202379183 submitted by Hokkaido University, which covers the preparation of the mesoscopic particles. The authors declare no other competing interests.

Acknowledgements

This work was supported by JSPS KAKENHI (23H01781 to V. B., 21H01753 to Y. T., 24H00445 to S. T., 22H04926 to ABiS), JSPS Core-to-Core Program for Advanced Research Network, JSPS Cooperative Research Program of "NJRC Mater. & Dev.", MEXT ARIM (JPMXP1223HK0009) and, International Priority Graduate Program (213073 to R. A.). P. M. and N. K. thank the ARC for support under grant CE170100026. We thank the Nikon Imaging Center at Hokkaido University for technical support on imaging, Dr H. Mitomo, Ms C. Takeuchi, and Dr K. Hirai for technical support on DLS and FT-IR measurements.

Notes and references

1 *Semiconductor Nanocrystal Quantum Dots*, ed. A. L. Rogach, Springer Vienna, Vienna, 2008.
2 G. H. Carey, A. L. Abdelhady, Z. Ning, S. M. Thon, O. M. Bakr and E. H. Sargent, *Chem. Rev.*, 2015, **115**, 12732–12763.
3 V. Biju, *Chem. Soc. Rev.*, 2014, **43**, 744–764.
4 J. Sobhanan, J. V. Rival, A. Anas, E. Sidharth Shibu, Y. Takano and V. Biju, *Adv. Drug Delivery Rev.*, 2023, **197**, 114830.
5 A. I. Ekimov, A. L. Efros and A. A. Onushchenko, *Solid State Commun.*, 1985, **56**, 921–924.
6 Y. Wang and N. Herron, *J. Phys. Chem.*, 1991, **95**, 525–532.
7 T. Takagahara and K. Takeda, *Phys. Rev. B: Condens. Matter Mater. Phys.*, 1992, **46**, 15578–15581.
8 C. B. Murray, D. J. Norris and M. G. Bawendi, *J. Am. Chem. Soc.*, 1993, **115**, 8706–8715.

9 J. Jasieniak and P. Mulvaney, *J. Am. Chem. Soc.*, 2007, **129**, 2841–2848.
10 A. P. Litvin, I. V. Martynenko, F. Purcell-Milton, A. V. Baranov, A. V. Fedorov and Y. K. Gun'Ko, *J. Mater. Chem. A*, 2017, **5**, 13252–13275.
11 L. E. Brus, *J. Chem. Phys.*, 1984, **80**, 4403–4409.
12 J. J. Urban, D. V. Talapin, E. V. Shevchenko and C. B. Murray, *J. Am. Chem. Soc.*, 2006, **128**, 3248–3255.
13 S. Mayilo, J. Hilhorst, A. S. Susha, C. Höhl, T. Franzi, T. A. Klar, A. L. Rogach and J. Feldmann, *J. Phys. Chem. C*, 2008, **112**, 14589–14594.
14 J. Grzyb, K. Walczewska-Szewc, J. Sławski and M. Trojnar, *Phys. Chem. Chem. Phys.*, 2021, **23**, 24505–24517.
15 B. C. Das, S. K. Batabyal and A. J. Pal, *Adv. Mater.*, 2007, **19**, 4172–4176.
16 X. He, Z. Li, M. Chen and N. Ma, *Angew. Chem., Int. Ed.*, 2014, **53**, 14447–14450.
17 M. S. Kodaimati, S. Lian, G. C. Schatz and E. A. Weiss, *Proc. Natl. Acad. Sci. U. S. A.*, 2018, **115**, 8290–8295.
18 H. Lv, C. Wang, G. Li, R. Burke, T. D. Krauss, Y. Gao and R. Eisenberg, *Proc. Natl. Acad. Sci. U. S. A.*, 2017, **114**, 11297–11302.
19 H. Tahara, M. Sakamoto, T. Teranishi and Y. Kanemitsu, *Nat. Nanotechnol.*, 2024, DOI: **10.1038/s41565-024-01601-9**.
20 R. Koole, P. Liljeroth, C. De Mello Donegá, D. Vanmaekelbergh and A. Meijerink, *J. Am. Chem. Soc.*, 2006, **128**, 10436–10441.
21 X. Xu, S. Stöttinger, G. Battagliarin, G. Hinze, E. Mugnaioli, C. Li, K. Müllen and T. Basché, *J. Am. Chem. Soc.*, 2011, **133**, 18062–18065.
22 J. Liu, X. Yang, K. Wang, X. He, Q. Wang, J. Huang and Y. Liu, *ACS Nano*, 2012, **6**, 4973–4983.
23 R. Schreiber, J. Do, E.-M. Roller, T. Zhang, V. J. Schüller, P. C. Nickels, J. Feldmann and T. Liedl, *Nat. Nanotechnol.*, 2014, **9**, 74–78.
24 D. X. Chen, Y. L. Sun, Y. Zhang, J. Y. Cui, F. Z. Shen and Y. W. Yang, *RSC Adv.*, 2013, **3**, 5765–5768.
25 M. Yamauchi and S. Masuo, *Chem. - Eur. J.*, 2020, **26**, 7176–7184.
26 J. Liu, K. Enomoto, K. Takeda, D. Inoue and Y.-J. Pu, *Chem. Sci.*, 2021, **12**, 10354–10361.
27 R. Huber and W. Bode, *Acc. Chem. Res.*, 1978, **11**, 114–122.
28 K. Ozawa and M. Laskowski, *J. Biol. Chem.*, 1966, **241**, 3955–3961.
29 J. V. Olsen, S. E. Ong and M. Mann, *Mol. Cell. Proteomics*, 2004, **3**, 608–614.
30 J. Zhuang, J. Zhang, M. Wu and Y. Zhang, *Adv. Sci.*, 2019, **6**, 1901462.
31 W. Deng, P. Chen, P. Hu, Z. He, M. Zhang, X. Yuan and K. Huang, *Sens. Actuators, B*, 2019, **292**, 180–186.
32 Y. Imry, *Introduction to mesoscopic physics*, Oxford University PressOxford, 2001.
33 A. Yella, H. W. Lee, H. N. Tsao, C. Yi, A. K. Chandiran, M. K. Nazeeruddin, E. W. G. Diau, C. Y. Yeh, S. M. Zakeeruddin and M. Grätzel, *Science*, 2011, **334**, 629–634.
34 R. F. Service, *Science*, 2012, **335**, 1167.
35 N. Nakatsuji, *Biomater. Sci.*, 2013, **1**, 9–10.
36 Y. Takakura and Y. Takahashi, *J. Controlled Release*, 2022, **350**, 486–493.
37 M. A. Shenashen, D. Hassen, S. A. El-Safty, M. M. Selim, N. Akhtar, A. Chatterjee and A. Elmarakbi, *Adv. Mater. Interfaces*, 2016, **3**, 1–12.
38 G. Wan, Y. Cheng, J. Song, Q. Chen, B. Chen, Y. Liu, S. Ji, H. Chen and Y. Wang, *Chem. Eng. J.*, 2020, **380**, 122458.
39 K. Boldt, N. Kirkwood, G. A. Beane and P. Mulvaney, *Chem. Mater.*, 2013, **25**, 4731–4738.
40 D. Sinclair and V. K. La Mer, *Chem. Rev.*, 1949, **44**, 245–267.
41 K. Barnham, J. L. Marques, J. Hassard and P. O'Brien, *Appl. Phys. Lett.*, 2000, **76**, 1197–1199.
42 S. Cherian and C. C. Wamser, *J. Phys. Chem. B*, 2000, **104**, 3624–3629.
43 Y. Wang, J. Sun, H. Zhang, Z. Zhao and W. Liu, *Catal. Sci. Technol.*, 2018, **8**, 2578–2587.
44 C. Rodríguez-Abreu, Y. V. Kolen'ko, K. Kovnir, M. Sanchez-Dominguez, R. G. Shrestha, P. Bairi, K. Ariga and L. K. Shrestha, *Phys. Chem. Chem. Phys.*, 2020, **22**, 23276–23285.
45 Y. Takano, T. Numata, K. Fujishima, K. Miyake, K. Nakao, W. D. Grove, R. Inoue, M. Kengaku, S. Sakaki, Y. Mori, T. Murakami and H. Imahori, *Chem. Sci.*, 2016, **7**, 3331–3337.
46 Satrialdi, R. Munechika, V. Biju, Y. Takano, H. Harashima and Y. Yamada, *Chem. Commun.*, 2020, **56**, 1145–1148.
47 T. Eralp, A. Shavorskiy and G. Held, *Surf. Sci.*, 2011, **605**, 468–472.
48 H. Zhao, R. Naganawa, Y. Yamada, Y. Osakada, M. Fujitsuka, H. Mitomo, Y. Miyatake, H. Harashima, V. Biju and Y. Takano, *J. Photochem. Photobiol., A*, 2024, **449**, 115397.
49 C. Flors, *J. Exp. Bot.*, 2006, **57**, 1725–1734.
50 H. Zhao, Y. Takano, D. Sasikumar, Y. Miyatake and V. Biju, *Chem. – Eur. J.*, 2022, **28**, e20220201.
51 A. E. Frise, E. Edri, I. Furó and O. Regev, *J. Phys. Chem. Lett.*, 2010, **1**, 1414–1419.
52 J. S. Kim, K. S. Song, J. H. Lee and I. J. Yu, *Arch. Toxicol.*, 2011, **85**, 1499–1508.
53 C. Wang, Z. Wang and X. Zhang, *Acc. Chem. Res.*, 2012, **45**, 608–618.
54 J. Sobhanan, Y. Takano, S. Sugino, E. Hirata, S. Yamamura and V. Biju, *NPG Asia Mater.*, 2022, **14**, 3.
55 B. Xie, L. Ma, J. Zhao and L. Liu, *Opt. Express*, 2019, **27**, A280.
56 T. He, X. Qiu, J. Li, G. Pang, Z. Wu, J. Cheng, Z. Zhou, J. Hao, H. Liu, Y. Ni, L. Li, X. Lin, W. Hu, K. Wang and R. Chen, *Nanoscale*, 2019, **11**, 15245–15252.
57 E. Hirata, Y. Takano, D. Konishi, Y. Maeda, N. Ushijima, M. Yudasaka and A. Yokoyama, *Chem. Commun.*, 2023, **59**, 11000–11003.
58 A. Tchoryk, V. Taresco, R. H. Argent, M. Ashford, P. R. Gellert, S. Stolnik, A. Grabowska and M. C. Garnett, *Bioconjugate Chem.*, 2019, **30**, 1371–1384.
59 Y. Lai, C. Xie, Z. Zhang, W. Lu and J. Ding, *Biomaterials*, 2010, **31**, 4809–4817.

